Article

A Non-MLE Approach for Satellite Scatterometer Wind Vector Retrievals in Tropical Cyclones

Suleiman Alsweiss [1],*, Rafik Hanna [2], Peth Laupattarakasem [2], W. Linwood Jones [2], Christopher C. Hennon [3] and Ruiyao Chen [2]

[1] Global Science & Technology Inc., 7855 Walker Drive, Suite 200, Greenbelt 20770, MD, USA
[2] Central Florida Remote Sensing Laboratory, Department of Electrical Engineering and Computer Science, University of Central Florida, Orlando 32816-2450, FL, USA;
E-Mails: rhyhanna1@yahoo.com (R.H.); plaupat@gmail.com (P.L.);
ljones5@cfl.rr.com (W.L.J.); chenruiyao@gmail.com (R.C.)
[3] Department of Atmospheric Sciences, University of North Carolina at Asheville, One University Heights, Asheville 28804, NC, USA; E-Mail: chennon@unca.edu

* Author to whom correspondence should be addressed; E-Mail: suleimanalsweiss@gmail.com.

Abstract: Satellite microwave scatterometers are the principal source of global synoptic-scale ocean vector wind (OVW) measurements for a number of scientific and operational oceanic wind applications. However, for extreme wind events such as tropical cyclones, their performance is significantly degraded. This paper presents a novel OVW retrieval algorithm for tropical cyclones which improves the accuracy of scatterometer based ocean surface winds when compared to low-flying aircraft with *in-situ* and remotely sensed observations. Unlike the traditional maximum likelihood estimation (MLE) wind vector retrieval technique, this new approach sequentially estimates scalar wind directions and wind speeds. A detailed description of the algorithm is provided along with results for ten QuikSCAT hurricane overpasses (from 2003–2008) to evaluate the performance of the new algorithm. Results are compared with independent surface wind analyses from the National Oceanic and Atmospheric Administration (NOAA) Hurricane Research Division's H*Wind surface analyses and with the corresponding SeaWinds Project's L2B-12.5 km OVW products. They demonstrate that the proposed algorithm extends the SeaWinds capability to retrieve wind speeds beyond the current range of approximately 35 m/s (minimal hurricane category-1) with improved wind direction accuracy, making this new approach a potential candidate for current and future conically scanning scatterometer wind retrieval algorithms.

1. Introduction

Over the past two decades, scientific and operational users have come to rely more on satellite remote sensing to provide vital measurements of geophysical parameters for weather and climate applications. Spaceborne scatterometers have been highly successful in measuring global synoptic ocean winds under all-weather, day/night conditions with high spatial and temporal sampling [1]. Currently, scatterometers are the major source of ocean surface vector wind (OVW) measurements, which are an intrinsic part of numerical weather forecasting and marine weather warning processes associated with extreme oceanic weather events such as tropical cyclones (TCs) [2].

Further, the use of satellite scatterometry for monitoring TCs has been significantly improved since the launch of the SeaWinds onboard the National Aeronautics and Space Administration's (NASA) QuikSCAT satellite in 1999. Fortunately, with the SeaWinds conically scanning pencil-beam antenna configuration, it was possible to produce wide-swath surface images of normalized radar cross sections (σ^0) at multiple azimuth angles. The resulting contiguous swath, not including the objectionable "nadir gap" found in prior NASA fan-beam scatterometers [3], offered a significant improvement in Earth coverage, and promoted a wider acceptance of QuikSCAT data for monitoring extreme weather events.

Despite the many successes scatterometers have achieved, measuring ocean surface winds in TCs with the presence of heavy precipitation remains a challenge that impairs their performance. Rain can affect the scatterometer measured σ^0 at the top of the atmosphere in three different ways. First, rain attenuates both the transmitted radar signal and the radar echo from the ocean surface. Second, rain produces its own volume backscatter due to scattering from rain drops in the atmosphere [4]. Third, rain striking the ocean roughens its surface, and imposes some (possibly highly nonlinear) modulation on the surface backscatter cross section [5].

Usually, satellite scatterometers operating frequencies are at Ku-band (~13 GHz) or C-band (~5 GHz). While both systems perform well in rain-free conditions, Ku-band scatterometers are much more susceptible to rain. When rain effects dominate the measured σ^0 values, spaceborne Ku-band scatterometer retrievals have consistently underestimated TC peak wind speeds, and they tend to retrieve unrealistic cross-swath wind directions (*i.e.*, are independent of the true wind direction and perpendicular to the instrument nadir track) [6].

This paper introduces a novel OVW retrieval algorithm, hereafter referred to as the eXtreme Winds retrieval algorithm (X-Winds) that is especially tailored to TCs. As a proof of concept, X-Winds was validated using data from SeaWinds on QuikSCAT. It has the potential to be applied to any conically scanning scatterometer such as the OceanSat-2 Scanning Scatterometer (OSCAT) launched by the Indian Space Research Organization (ISRO) in September 2009, or the upcoming RapidSCAT scatterometer to be installed on the International Space Station (ISS) in 2014.

To evaluate the performance of X-Winds, 10 different case studies of several storms are compared with independent National Oceanic and Atmospheric Administration (NOAA) Hurricane Research Division's (HRD) H*Wind surface winds analyses [7], and with NASA's SeaWinds Project standard L2B 12.5 km OVW product (hereafter referred to as L2B-12.5 km).
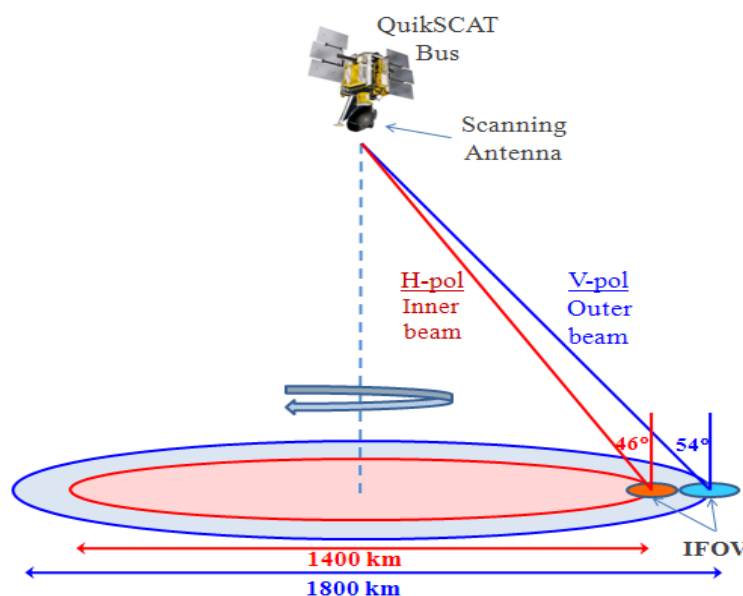
The remaining of the paper is organized as follows: Section 2 contains an overview of the SeaWinds instrument and the datasets used, and then algorithm description followed by results and algorithm evaluation are presented in Sections 3 and 4, respectively.

2. Instrument and Data Overview

2.1. SeaWinds Overview

SeaWinds on QuikSCAT was a Ku-band (13.4 GHz) scatterometer with a conically scanning parabolic reflector antenna, operating with two-beams at two different earth incidence angles (outer vertically polarized (V-pol) beam at 54 ° earth incident angle and inner horizontally polarized (H-pol) beam at 46 ° earth incident angle) [8]. Radar backscatter measurements were obtained over the full 360 ° of azimuth sampling a wide swath (1800 km for outer beam, and 1400 km for inner beam) on the Earth's surface as illustrated in Figure 1.

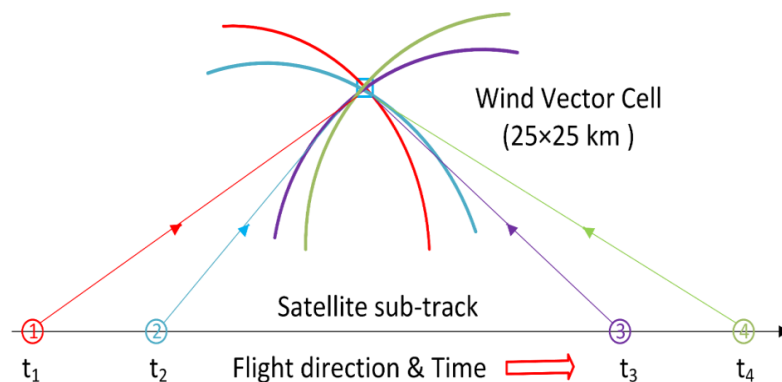**Figure 1.** QuikSCAT conically scanning measurement geometry.

The SeaWinds multi-look σ^0 measurements (*i.e.*, pointing forward and aft at two different polarizations), also known as flavors, were grouped into latitude/longitude grids called wind vector cells (WVCs). These grouped σ^0 observations were then used in the SeaWinds geophysical retrieval algorithm to infer neutral stability wind vectors at 10-m height above the ocean surface [9].

2.2. SeaWinds Measurements and Data Products

SeaWinds' conical scan geometry was designed to provide overlapping measurements from two beams (looking both forward and aft) and results in four azimuth looks at each WVC. Since σ^0 is anisotropic with wind direction, obtaining multi-azimuth looks allows the inference of surface wind speeds and directions using a geophysical model function (GMF), which maps σ^0 to wind speed and relative wind direction (χ), via an inversion algorithm [10].

For instance, consider the WVC shown in Figure 2. Ocean backscatter is first measured by the outer beam (V-pol) during the forward scan portion at time t_1 (red arc). This is shortly followed by the inner beam (H-pol) forward scan at t_2 (blue arc). A few minutes later, a measurement is made from the inner beam from aft scan segment at t_3 (purple arc). Finally, the outer beam aft-look is measured at t_4 (green arc).

Figure 2. Time sequence of QuikSCAT measuring 4-flavor radar backscatter at one wind vector cell location. Each arc represents a portion of conical scan series of measurements.

The SeaWinds measured σ^0 on a pulse-by-pulse basis in range-slices of ~4 km each. These multi-pulse range-sliced backscatter powers are grouped in WVCs and stored in the SeaWinds L2A data product. Another useful parameter included in the L2A data product is the simultaneous QuikSCAT Radiometer (QRad) V- and H-pol ocean brightness temperatures (Tbs) derived from the SeaWinds antenna noise measurements [11].

Moreover, QuikSCAT retrieved winds used here are from the L2B data. They are derived from L2A backscatter using the empirical QSCAT-1 GMF [12] and MLE as the inversion algorithm to select the most probable wind vector solution. To improve wind direction in the middle of the swath, where azimuth diversity is poor, the Direction Interval Retrieval with Threshold Nudging (DIRTH) algorithm is applied. This retrieval technique provides approximately 2 m/s and 20° accuracy in wind speed and direction, respectively [13,14].

Since July 2006, SeaWinds Level 2 data products (L2A and L2B), provided by the Jet Propulsion Laboratory (JPL), have been available at two spatial resolutions (25 km and 12.5 km) on a spacecraft grid of cross-track WVCs. Because of the improved spatial resolution of the SeaWinds 12.5 km products (L2A-12.5 km and L2B-12.5 km), they offered an advantage for hurricane observations, hence used for the wind retrieval results presented herein.

Both L2A and L2B data products are provided by NASA Physical Oceanography Distributed Active Archive Center (PODAAC) facility at JPL, and further information can be found online at ftp://podaac.jpl.nasa.gov/ocean_wind/quikscat/L2B/doc/QSUG_v3.pdf.

2.3. H*Wind Surface Wind Analyses

H*Wind [7] is an objective surface wind analyses tool that assimilates all available wind observations from a specified time period to produce the best possible depiction of the instantaneous surface winds of a TC. Typical datasets incorporated into an analysis include: satellite observations, aircraft reconnaissance flight-level winds translated to surface values, *in-situ* wind vector from global positioning system (GPS) dropsondes from aircrafts, surface wind speed and rain rate from the Stepped Frequency Microwave Radiometer (SFMR), and buoy/ships surface wind speeds and directions.

H*Wind produces a 6-km resolution, 2-dimensional, gridded, one-minute sustained wind speed and direction field at a 10-m reference height. The most accurate H*Wind fields are obtained when aircraft reconnaissance and/or SFMR data are extensively used in the analysis. A comprehensive H*Wind error analysis for those cases shows that the total uncertainty in a hurricane H*Wind analysis is 6% near the storm center and increases to 13% near the radius of tropical storm force winds [15]; this makes H*Wind the most reliable observation-based OVW currently available in a hurricane environment.

3. The X-Winds Hurricane Retrieval Algorithm

The X-Winds retrieval algorithm performs a separate (two-step) wind direction (*wd*) and wind speed (*ws*) estimates. This differs from the conventional MLE based ocean wind vector retrievals where wind speeds and directions are found simultaneously. A detailed description of the X-Winds OVW retrieval algorithm follows.
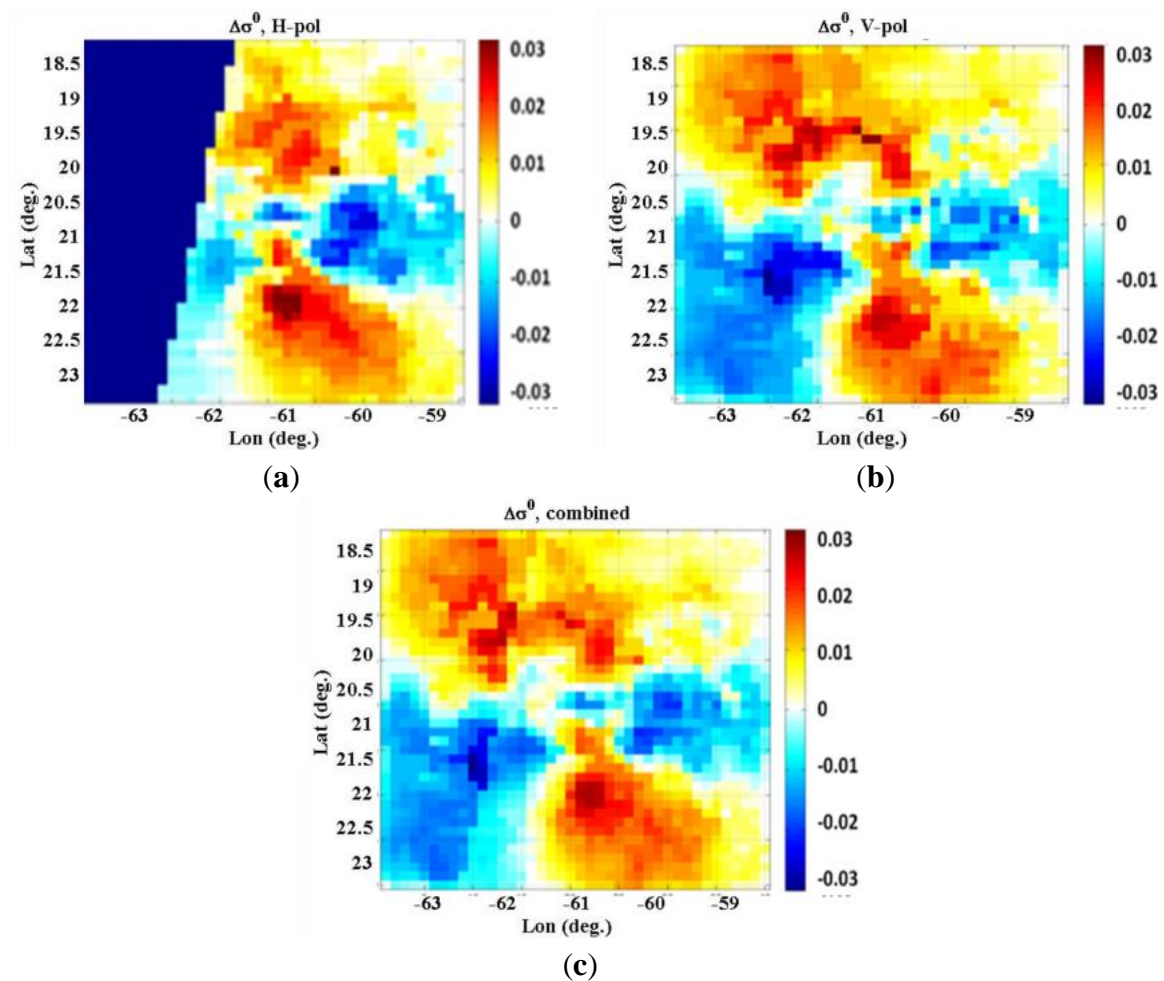
3.1. Modeling Wind Direction Signature in Ocean Backscatter

Using SeaWinds L2A-12.5 km data, we calculated the difference between forward and aft σ^0 measurements ($\Delta\sigma^0_{Meas}$) obtained from multiple azimuth observations for a given polarization. Figure 3 shows typical hurricane $\Delta\sigma^0_{Meas}$ images from Hurricane Fabian (a $5° \times 5°$ latitude/longitude box around the storm center on a relative scale of $0.125°$ (~12.5 km) increments) for: (a) H-pol, (b) V-pol, and (c) the average of both polarizations, generated from the L2A-12.5 km product. Although the dynamic range of σ^0 is different for H- and V-pol, the relative difference between forward and aft looks is found to be very similar.

It is noted that these $\Delta\sigma^0_{Meas}$ images exhibit a robust 4-quadrant nature that is representative of relative wind direction. In addition, these images do not show the patterns of spiral rain bands, usually found in TCs, although they are clearly visible in the individual σ^0 looks images. This $\Delta\sigma^0_{Meas}$ effect is the result of the rain attenuation being nearly isotropic when averaged over the WVC. Because of slightly different rain in the forward and aft looks, the rain attenuations are not identical; yet, the magnitude of the rain attenuation difference is small compared to the wind direction anisotropy.

As a result, $\Delta\sigma_{Meas}^0$ is mainly due to the different wind directions relative to antenna azimuth (χ) obtained from different looks.

Figure 3. Observed ocean backscatter difference ($\Delta\sigma_{Meas}^0$, (forward-aft looks)) from Hurricane Fabian (Rev. # 21898) for: (**a**) horizontal polarization, (**b**) vertical polarization, and (**c**) average of horizontal and vertical polarizations.

(**a**)

(**b**)

(**c**)

In general, ocean radar backscatter at the top of the atmosphere can be modeled as a second harmonic Fourier series of χ and a set of coefficients (c_0, c_1, and c_2) that are functions of wind speed (*ws*) as shown in Equation (1) [16–18]. The three c_i coefficients shape the model's wind speed and directional dependence and are empirically derived.

$$\sigma_{Mod}^0 = c_0(ws) + c_1(ws)\cos(\chi) + c_2(ws)\cos(2\chi) \tag{1}$$

Using Equation (1), the modeled σ^0 difference ($\Delta\sigma_{Mod}^0$) is mathematically expressed in Equations (2a) and (2b), and can be expanded to Equation (2c) using trigonometric identities and substituting χ_{For} with ($\psi_{For} - wd$) and χ_{Aft} with ($\psi_{Aft} - wd$), where ψ_{For} and ψ_{Aft} are the forward and aft measurements azimuth angles respectively:

$$\Delta\sigma_{Mod}^0 = \sigma_{For}^0 - \sigma_{Aft}^0 \tag{2a}$$

$$\Delta\sigma_{Mod}^0 = c_1[cos(\chi_{For})] + c_2[cos(2\chi_{For})] - c_1[cos(\chi_{Aft})] - c_2[cos(2\chi_{Aft})] \tag{2b}$$

$$\Delta\sigma_{Mod}^0 = c_1[cos(\psi_{For})\,cos(wd) + sin(\psi_{For})\,sin(wd)]$$
$$+ c_2[cos(2\psi_{For})\,cos(2wd) + sin(2\psi_{For})\,sin(2wd)]$$
$$- c_1[cos(\psi_{Aft})\,cos(wd) + sin(\psi_{Aft})\,sin(wd)]$$
$$- c_2[cos(2\psi_{Aft})\,cos(2wd) + sin(2\psi_{Aft})\,sin(2wd)] \tag{2c}$$

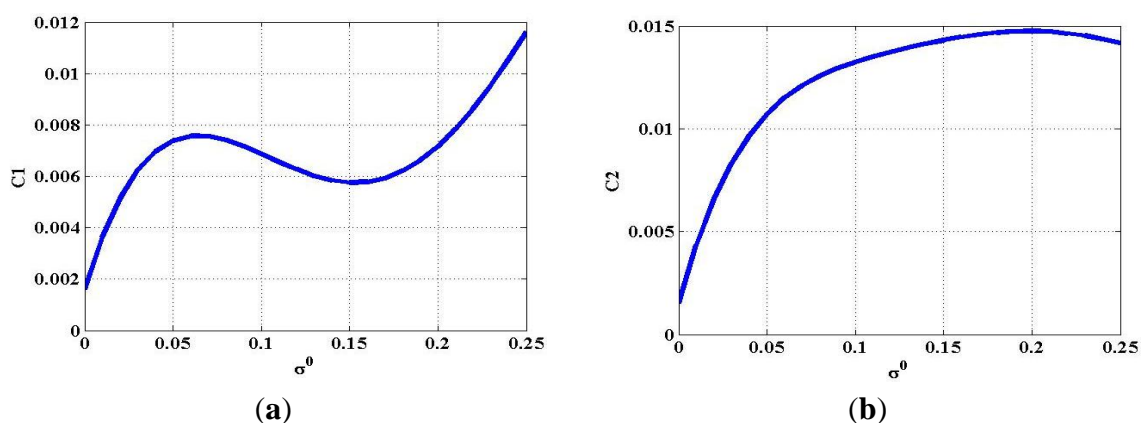Substituting the trigonometric identities from Equations (3a) and (3b) in Equation (2c) yields to Equation (4):

$$cos(2x) = 2\cos^2(x) - 1 \tag{3a}$$

$$sin(x) = \pm\sqrt{1 - \cos^2(x)} \tag{3b}$$

$$\Delta\sigma_{Mod}^0 = c_2\,[2cos(2\psi_{For})\cos^2(wd) - 2cos(2\psi_{Aft})\cos^2(wd)$$
$$+ 2sin(2\psi_{For})\sqrt{1 - \cos^2(wd)}\,cos(wd) - 2\,sin(2\psi_{Aft})\sqrt{1 - \cos^2(wd)}\,cos(wd)$$
$$- c_2\,cos(2\psi_{For}) + c_2cos(2\psi_{Aft})] \tag{4}$$
$$+ c_1\,[cos(\psi_{For})\,cos(wd) - cos(\psi_{Aft})\,cos(wd) + sin(\psi_{For})\sqrt{1 - \cos^2(wd)}$$
$$- sin(\psi_{Aft})\sqrt{1 - \cos^2(wd)}\,]$$

To solve Equation (4), it is necessary to estimate c_1 and c_2, which are functions of the unknown wind speed. While all three c_i coefficients have wind speed dependence, the dominant wind speed signature in σ^0 is captured by the c_0 term. Thus, using the direct mapping of wind speed and σ^0 in the c_0 term, the average of the forward and aft σ^0 measurements was taken as a proxy for the mean wind speed. If the forward and aft looks were separated by 90°, then their average would be nearly equal to the isotropic normalized cross section c_0 and thereby independent of swath position. However, because of the QuikSCAT geometry, the relative azimuth between forward and aft looks varies with the measurement location in the swath; a minor variability of these coefficients with the WVC position is expected but has not been fully investigated. For simplicity, this effect was ignored, and the coefficients presented in Figure 4 are an average across the swath. This will be addressed in future algorithm improvements by providing these coefficients *versus* WVC position and assessing their impact on both wind direction and wind speed retrievals uncertainty.

Figure 4. The coefficients (**a**) c_1 and (**b**) c_2 used to retrieve wind direction.

(**a**) (**b**)

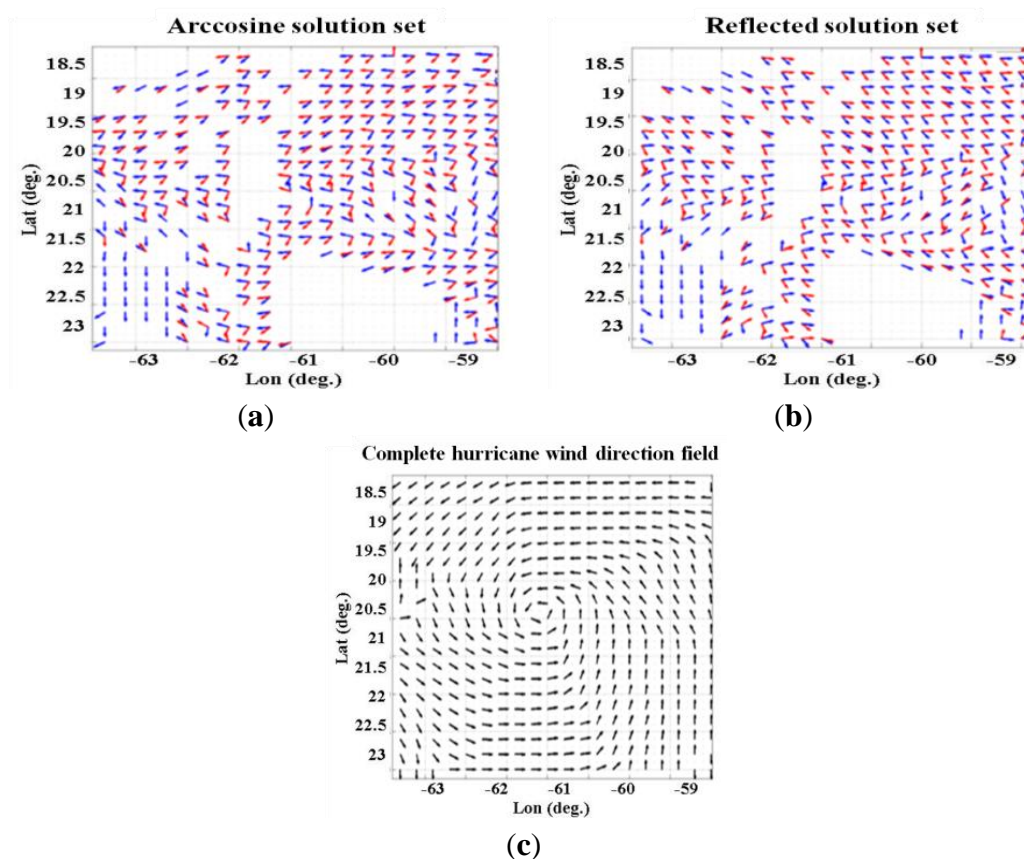Therefore, given ψ_{For} and ψ_{Aft} (from the L2A-12.5 km data) and c_1, and c_2 (from Figure 4), Equation (4) can be simply expressed as in Equation (5):

$$\Delta\sigma^0_{Mod} = f(wd) \tag{5}$$

3.2. Wind Direction Retrieval

The wind direction retrieval is performed on a field-wise basis in a $5° \times 5°$ latitude/longitude box around the *a priori* storm center provided by NOAA's National Hurricane Center (NHC) "best track" location (determined post-storm by forecasters using all available data). Possible wind direction solutions for each WVC (also called wind direction aliases) [10,19] are estimated by finding the directions that minimize the objective function ($\Delta\sigma^0_{Meas} - \Delta\sigma^0_{Mod}$). This retrieval procedure involves the inversion of the arccosine function; thus the solutions are limited to the range between $0°$–$180°$ (Figure 5a). A mirror image of wind direction about the y-axis is implemented in order to extend wind direction to full $360°$ (Figure 5b).

Figure 5. X-Winds wind direction retrievals for Hurricane Fabian (Rev. # 21898): (**a**) is initial wind direction solutions, (**b**) is wind direction mirror image, and (**c**) is the complete hurricane wind direction silhouette after de-aliasing and interpolation.

(**a**) (**b**)

(**c**)

In scatterometer OVW retrievals, selecting the "true" wind direction from a number of candidate directions is a common problem [18,20]. Our wind alias removal technique involves an iterative procedure using a "first guess" counter clockwise spiral wind direction for TCs in the northern hemisphere (clockwise in the southern hemisphere) and median filtering. The first-pass uses

a 20 ° inward spiral wind direction model field around the known NHC storm center with a ±45 ° wind direction window to select candidate aliases. Next, a median filter is applied over a sliding spatial window of 3 × 3 WVCs to generate the median direction field. Because a solution to the arccosine only occurs if ($\triangle \sigma^0_{Meas} - \triangle \sigma^0_{Mod}$) is between −1 and 1, some WVCs have no solution due to erroneous or highly contaminated measurements. These WVCs with no solution are filled by interpolation to complete hurricane wind direction silhouette field depicted in Figure 5c. A quality flag is generated to identify the interpolated WVCs as low quality retrievals with compromised accuracy.
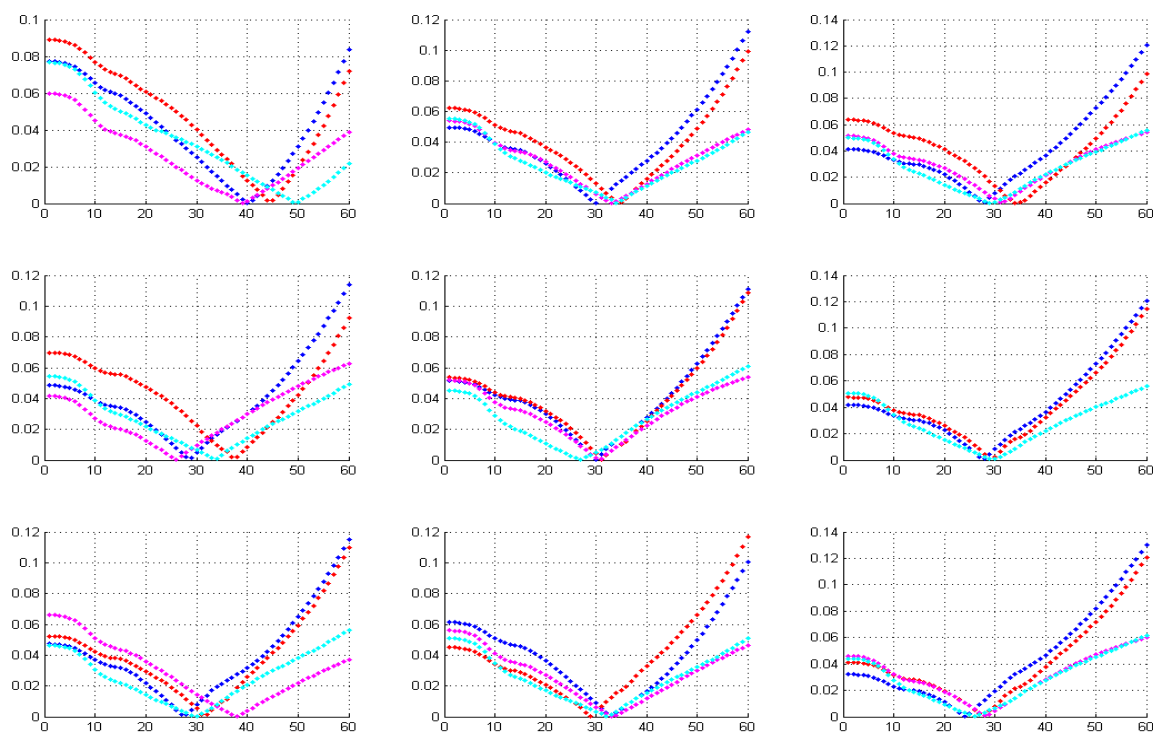
3.3. Wind Speed Retrieval

With wind directions in hand, this reduces the complexity of the inversion process to one dimension; hence, wind speeds can be computed directly from the GMF given the now known wind directions. Wind speeds of each flavor are retrieved individually by searching for the wind speed value that minimizes the absolute difference between L2A-12.5 km measured σ^0 (σ^0_{Meas}) and modeled σ^0 (σ^0_{GMF}), computed from Equation (6):

$$\sigma^0_{GMF} = GMF(ws, \chi, p, f, \theta, TbH) \tag{6}$$

where polarization (*p*), operating frequency (*f*), and incidence angle (*θ*), are based on the QuikSCAT configuration, and *χ* is obtained from the SeaWinds measurement azimuth and the retrieved wind direction (from Section 3.2), leaving (*ws*) as the only unknown.

Figure 6. Wind speeds retrieval for a window of a 3 × 3 wind vector cells. X-axes are retrieved wind speeds (m/s), and y-axes are the absolute difference between measured and modeled radar backscatter ($\sigma^0_{Meas} - \sigma^0_{GMF}$). Color indicates different σ^0 flavors.

H-pol forward look, H-pol aft look, V-pol forward look, V-pol aft look.

An example of wind speed retrievals is shown in Figure 6 for a region comprising of 3×3 WVCs (9 panels). The retrieved wind speed from each flavor (distinguished by different color) occurs when the difference of σ_{Meas}^0 and σ_{GMF}^0 is at a minimum. The retrieved wind speed for any individual WVC is the average of all wind speeds obtained from available flavors after being passed through a 3×3 low pass filter to suppress noise. Averaging wind speeds retrieved from all available flavors is expected to reduce wind direction error propagation on the wind speed retrieval. It is important to note that our technique cannot compensate for the lower wind speed retrievals caused by σ^0 rain attenuation. On the other hand, when using the MLE technique, typical rain attenuation causes significant errors in both the wind direction and wind speed retrievals, and the resulting wind speed is strongly affected by the wind direction error. Overall our approach reduces the effect of rain attenuation and results in smaller wind speed error compared to the conventional MLE approach.

4. Results and Performance Evaluation

The performance of the new X-Winds algorithm was assessed using 10 QuikSCAT hurricane overpasses (listed in Table 1) with collocated H*Wind analyses as the assumed "surface truth". The H*Wind analyses used in assessing X-Winds were created without including QuikSCAT data to insure independence, and they were spatially interpolated to the SeaWinds L2B-12.5 km WVC locations.

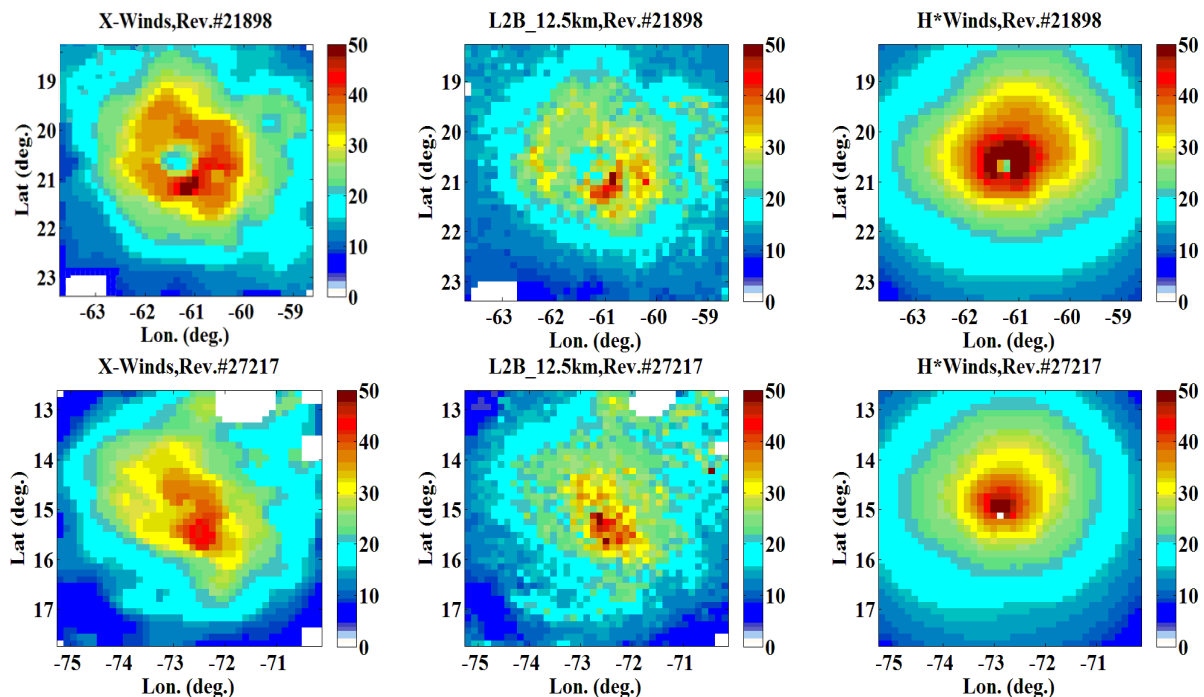**Table 1.** QuikSCAT hurricane overpasses used to evaluate X-Winds algorithm.

Hurricane Name	Hurricane Date(mm/dd/yyyy)	SeaWinds Rev. #
Fabian	09/01/2003	21877
Fabian	09/02/2003	21898
Isabel	09/10/2003	22005
Ivan	09/09/2004	27217
Ivan	09/12/2004	27253
Cindy *	07/05/2005	31481
Bertha	07/11/2008	47194
Gustav	08/31/2008	47915
Ike	09/06/2008	48000
Ike	09/06/2008	48007

* Cindy was a strong tropical storm (maximum sustained wind = 60 kt).

4.1. X-Winds Wind Speed Evaluation

In this subsection; retrieved wind speeds are compared to QuikSCAT L2B-12.5 km product when both were evaluated with the HRD H*Wind surface analyses as the assumed "surface truth". For qualitative comparisons; two examples of typical hurricane fields are presented in Figure 7. The top panels are the QuikSCAT descending revolution that observed the category-4 Hurricane Fabian in September 2003; and the lower panels are category-4 Hurricane Ivan in September 2004. Each hurricane image represents a $5° \times 5°$ gridded box centered on the hurricane eye. Wind speed images are presented in the same color scale ranging from 0 to 50 m/s corresponding to low hurricane catetory-3 force wind.

Figure 7. Surface wind speeds for Hurricane Fabian (upper panels) and Hurricane Ivan (lower panels). Color indicates wind speeds from 0–50 m/s. Left panels are X-Winds retrievals, center panels are JPL L2B-12.5 km, and right panels are H*Wind surface analyses.

In order to evaluate the overall wind speed retrieval performance of X-Winds, the statistical metrics are computed from composite data of the ten hurricane revolutions. Results are presented in Figure 8 as wind speed scatter plots of X-Winds (Figure 8a) and L2B-12.5 km (Figure 8b) compared to H*Wind (x-axis). Each point is a single WVC retrieval and the color corresponds to QRad TbH that is used to indicate rain intensity (warmer colors correspond to higher rain rates). This comparison shows that X-Winds can provide reliable wind speeds up to ~40 m/s without exhibiting saturation beyond 30 m/s (weak hurricane category-1).

Wind speed accuracy is further assessed by comparing the statistical performance of X-Winds and L2B-12.5 km for each H*Wind wind speed range (with a 10 m/s increment steps). For low wind speeds (<15 m/s, away from the center of the storm), both X-Winds and L2B-12.5 km look similar. This speaks well for X-Winds because L2B-12.5 km wind speeds (up to ~20 m/s) are known to be accurate within ~2 m/s [1,14]. For higher wind speeds, X-Winds is considerably more accurate than L2B-12.5 km. In particular, L2B-12.5 km underestimates wind speeds beyond hurricane force winds (>33 m/s) by >6 m/s, while X-Winds wind speed error is <3 m/s for wind speeds up to 60 m/s. The detailed statistics are summarized in Table 2.

Figure 8. Wind speed comparisons with H*Wind for composite of 10 QuikSCAT hurricane revolutions: (**a**) is X-Winds and (**b**) is L2B-12.5 km. Color scale denotes the QRad H-pol brightness temperature (warm colors indicate rain).
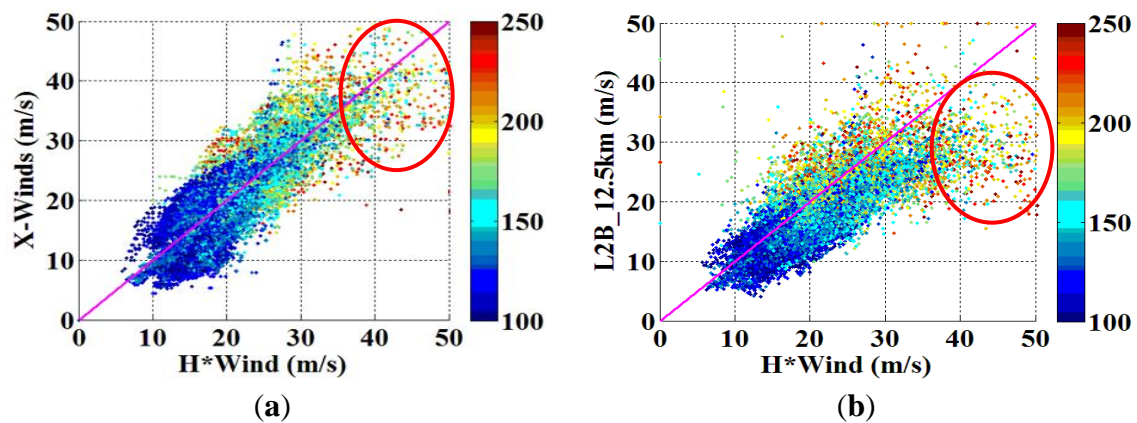

(**a**) (**b**)

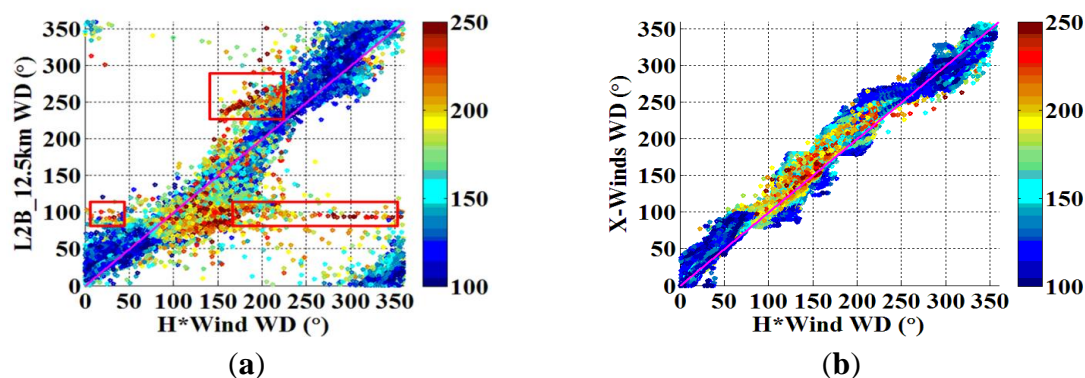**Table 2.** X-Winds and L2B-12.5 km wind speed error compared to H*Wind.

Wind Speeds (m/s)	Approximate Storm Class	X-Winds			L2B-12.5 km		
		Mean (m/s)	STD (m/s)	Correlation (r^2)	Mean (m/s)	STD (m/s)	Correlation (r^2)
10–20	Tropical depression	−3.0	2.8	0.65	−2.7	2.4	0.70
20–30	Tropical storm	0.1	3.0	0.94	−3.0	3.1	0.86
30–40	Hurricane Category-1	−0.4	3.3	0.90	−3.8	4.1	0.78
40–50	Hurricane Category-2	−1.6	4.4	0.94	−8.6	7.2	0.53
50–60	Hurricane Category-3	−2.56	6.4	0.83	N/A	N/A	N/A

4.2. X-Winds Wind Direction Evaluation

To further assess X-Winds performance, wind directions from X-Winds, L2B-12.5 km, and H*Wind were compared for the composite of the 10 QuikSCAT hurricane overpasses. The scatter plots in Figure 9 shows that both L2B-12.5 km (Figure 9a) and X-Winds (Figure 9b) wind directions agree reasonably well with H*Wind in non-raining regions (indicated by cold colors, where color scale denotes QRad TbH).

However, in the presence of rain (indicated by warm colors or higher TbH values), where σ^0 measurements are dominated by isotropic rain volume backscatter, the SeaWinds OVW algorithm retrieves cross-swath wind directions [4,19] (see "red boxes" in Figure 9a). In contrast, X-Winds rain effects tend to cancel (due to their isotropic nature) when subtracting the forward and aft azimuth looks to calculate the $\Delta\sigma^0_{meas}$ used to infer wind direction. Therefore, wind direction retrievals using the X-Winds algorithm are much less affected by rain contamination and thus retrieve more accurate winds. Figure 9b demonstrates how X-Winds' wind directions are in good correlation with H*Wind over the full 360 ° wind direction range.

Figure 9. Composite wind direction comparisons for ten hurricane cases: (**a**) L2B-12.5 km wind directions comparison with H*Wind, and (**b**) X-Winds' wind directions comparison with H*Wind. Color scale denotes the QRad TbH (warm colors indicate rain).

(**a**)   (**b**)

Moreover, retrieved wind direction accuracy of X-Winds and L2B-12.5 km for each H*Wind wind speed range (with a 10 m/s increment steps) was evaluated, and the detailed statistics are summarized in Table 3.

Table 3. X-Winds and L2B-12.5 km wind direction error compared to H*Wind.

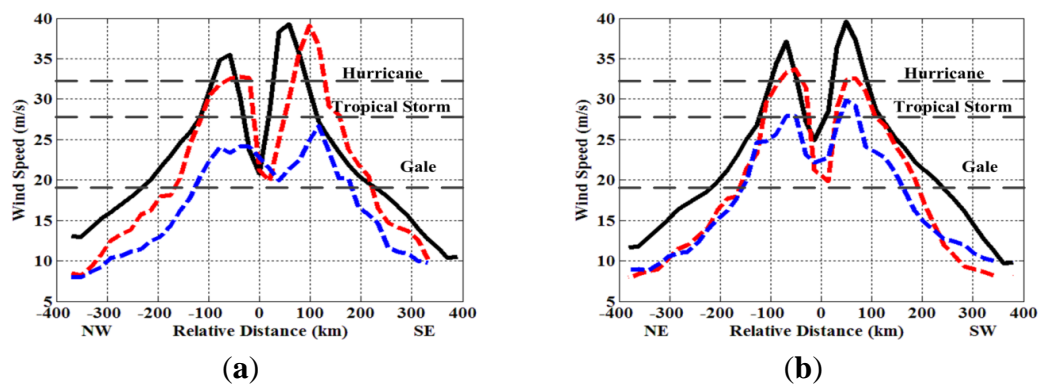| Wind Speeds (m/s)	Approximate Storm Class	X-Winds			L2B-12.5 km		
		Mean ($°$)	STD ($°$)	Correlation (r^2)	Mean ($°$)	STD ($°$)	Correlation (r^2)
10–20	Tropical depression	10.0	15.0	0.98	15.0	31.0	0.90
20–30	Tropical storm	9.0	16.0	0.99	16.0	40.0	0.82
30–40	Hurricane Category-1	11.0	19.0	0.99	13.0	46.0	0.72
40–50	Hurricane Category-2	11.0	23.0	0.98	20.0	38.0	0.65
50–60	Hurricane Category-3	10.0	24.0	0.98	N/A	N/A	N/A

4.3. X-Winds Wind Radii Measurements

Improvements in forecasts of wind radii could provide unprecedented societal benefits and serve as additional guidance for local emergency managers dealing with land falling TCs. In this section, we present the QuikSCAT radial wind speeds profiles based on X-Winds and L2B-12.5 km compared to H*Wind analyses.

Figure 10 shows this comparison for Hurricane Bertha Rev. # 47194 with NOAA operational wind speed thresholds shown as horizontal lines corresponding to gale-force (17 m/s), tropical storm-force (25 m/s), and hurricane force (33 m/s) winds. The QuikSCAT radial wind profiles are averaged by quadrant (X-Winds = dashed red lines and L2B-12.5 km = dashed blue lines) and are overlaid with H*Wind wind speed profile (solid black lines). The intersection of these profiles with wind speed thresholds determines the radii of gale, tropical storm and hurricane force winds with respect to the storm center. Figure 10a is the storm radial profiles from northwest-to-southeast, and Figure 10b is from northeast-to-southwest.

Unlike the L2B-12.5 km which consistently underestimate storm's wind speeds, X-Winds wind speed profiles agrees better with H*Wind. We believe that the disagreement inside the eye wall region

is due to heavy rain contamination and backscatter saturation effects, which prevent accurate wind speed measurements in the TC eye wall region. In addition, at distance greater than 100–200 km from the center, H*Wind analyses use interpolation/extrapolation to fill missing pixels beyond aircraft observations, and is unable to resolve smaller-scale/asymmetric wind features such as concentric eyewalls and rain bands [15].

Figure 10. Radial wind speed profiles averaged by quadrant for Hurricane Bertha Rev. # 47194. Panel-a represents diagonal profiles from northwest to southeast, and panel-b represents diagonal profiles from northeast to southwest. Solid black lines are H*Wind, dashed red lines are X-Winds, and dashed blue lines are L2B-12.5 km.

(**a**)　　　　　　　　　　(**b**)

5. Conclusions

SeaWinds on QuikSCAT has been shown to provide accurate measurement of global synoptic ocean surface wind vectors. However, under extreme weather conditions like TCs, it significantly understates the OVWs of the ocean surface. Both rain contamination and ocean radar backscatter saturation at high wind speeds can cause underestimation of measured wind speed by the traditional MLE based scatterometer OVW retrieval algorithms.

This paper presents a new technique, named eXtreme Wind retrieval algorithm or X-Winds, to mitigate conical scanning scatterometer limitations for OVW retrievals in TCs. X-Winds sequentially solves for scalar wind directions, using the relative difference of the radar backscatter observations from various azimuth looks, which is believed to be less sensitive to rain, and then uses these wind direction estimates to calculate the corresponding scalar wind speeds. While the present work suffers from a few approximations in the wind direction retrievals that have not been fully vetted in the current version of the algorithm, the statistical results show that this two-step scalar wind direction and subsequent wind speed retrieval algorithm is superior to the conventional MLE approach in hurricanes with significant rain attenuation effects. While both retrieval techniques suffer from the reduction of σ^0 due to rain attenuation, X-Winds has the apparent major strength of improved wind direction, which results in improved wind speed retrievals by minimizing the coupled wind direction errors associated with the MLE.

X-Winds wind speed and wind direction retrievals were evaluated using the NOAA Hurricane Research Division's H*Wind surface wind analyses as the most reliable assumed surface truth.

Comparisons with the SeaWinds standard JPL L2B-12.5 km OVW product for ten QuikSCAT hurricane validation cases during 2003–2008 are presented.

Results show that X-Winds OVW retrievals compare well in the mean with H*Wind speeds including wind speed regimes > ~30 m/s. Utilizing the same GMF used in generating the SeaWinds L2B data product, X-Winds is able to retrieve higher wind speeds around the TC eye wall where rain attenuation dominates (typically 5–8 m/s higher). Moreover, both X-Winds and L2B-12.5 km wind directions agree well with H*Wind for non-raining regions, while X-Winds wind directions were noticeably better in rain contaminated regions. These results suggest that X-Winds retrievals have improved upon previous OVW measurement shortcomings in hurricanes and have extended scatterometer capability to measure hurricane force winds.

Finally, while the X-Winds algorithm remains as work in progress, we believe that it can serve as a potential candidate for OVW retrieval algorithm for any current and future conically scanning scatterometer, e.g., OceanSat-2 Scatterometer and ISS-RapidSCAT, and will yield improved OVW retrievals in extreme wind events.

Author Contributions

This research was co-guided by W. Linwood Jones and Christopher Hennon. The idea of this work was mainly developed and discussed by Suleiman Alsweiss, Rafik Hanna and Peth Laupattarakasem. Ruiyao Chen helped in fine tuning the algorithm. All authors helped in revising and improving this paper, and responding to reviewers comments.

Conflicts of Interest

The authors declare no conflict of interest.

References

1. Chelton, D.; Freilich, M. Scatterometer-based assessment of 10-m wind analysis from the operational ECMWF and NCEP numerical weather prediction models. *Mon. Weather Rev.* **2005**, *133*, 409–429.
2. Chang, P.; Jelenak, Z. *NOAA Operational Ocean Surface Vector Winds Requirements Workshop*; Workshop Report; NOAA National Hurricane Center: Miami, FL, USA, 2006; Available online: http://manati.orbit.nesdis.noaa.gov/SVW_nextgen/SVW_workshop_report_final.pdf (accessed on 30 April 2014).
3. Jones, W.L.; Cardone, V.J.; Pierson, W.J.; Zec, J.; Rice, L.P.; Cox, A.; Sylvester, W.B. NSCAT high resolution surface winds measurements in typhoon violet. *J. Geophys. Res.* **1999**, *104* (Suppl. C5), 11247–11260.
4. Moore, R.K.; Yu, Y.S.; Fung, A.K; Kaneko, D.; Dome, G.; Werp, R. Preliminary study of rain effects on radar scattering from water surfaces. *IEEE J. Ocean. Eng.* **1979**, *OE-4*, 31–32.
5. Craeye, C. Study of Microwave Scattering from Rain and Wind Roughened Seas. Ph.D. Dissertation, Universite Catholique de Louvain, Louvain, Belgium, France, 1998.

6. Weissman, D.E.; Stiles, B.W.; Hristova-Veleva, S.M.; Long, D.G.; Smith, D.K.; Hilburn, K.A.; Jones, W.L. Challenges to satellite sensors of ocean winds: Addressing precipitation effects. *J. Atmos. Technol.* **2012**, *29*, 356–374.

7. Powell, M.D.; Houston, S.H.; Amat, L.R.; Morisseau-Leroy, N. The HRD real-time hurricane wind analysis system. *J. Wind Eng. Ind. Aerodyn.* **1998**, *77/78*, 53–64.

8. Spencer, M.W.; Wu, C.; Long, D.G. Improved resolution backscatter measurements with the SeaWinds pencil-beam scatterometer. *IEEE Trans. Geosci. Remote Sens.* **2000**, *38*, 89–104.

9. Liu, W.T.; Tang, W. *Equivalent Neutral Wind*; Jet Propulsion Lab. Pub. 96-17; Jet Propulsion Laboratory: Pasadena, CA, USA, 1996.

10. Naderi, F.M.; Freilich, M.H.; Long, D.G. Spaceborne radar measurement of wind velocity over the ocean—An overview of the NSCAT scatterometer system. *IEEE Trans. Geosci. Remote Sens.* **1991**, *79* (Suppl. 6), 850–866.

11. Ahmad, A.K.; Jones, W.L.; Kasparis, T.; Vergara, S.; Adams, I.S.; Park, J.D. Oceanic rain rate estimates from the QuikSCAT Radiometer: A global precipitation mission pathfinder. *J. Geophys. Res. Atmos.* **2005**, *110*, doi:10.1029/2004JD005560.

12. Jet Propulsion Laboratory (JPL). QuikSCAT Science Data Product User's Manual Overview & Geophysical Data Products. Available online: ftp://podaac-ftp.jpl.nasa.gov/allData/quikscat/L2B/v2/docs/QSUG_v3.pdf (accessed on 30 April 2014).

13. Stiles, B.W.; Pollard, B.D.; Dunbar, R.S. Direction interval retrieval with thresholded nudging: A method for improving the accuracy of QuikSCAT winds. *IEEE Trans. Geosci. Remote Sens.* **2002**, *40* (Suppl. 1), 79–89.

14. Ebuchi, N.; Graber, H.C.; Caruso, M.J. Evaluation of wind vectors observed by QuikSCAT/SeaWinds using ocean buoy data. *J. Atmos. Ocean. Technol.* **2002**, *19*, 2049–2069.

15. DiNapoli, S.M.; Bourassa, M.A.; Powell, M.D. Uncertainty and intercalibration analysis of H*Wind. *J. Atmos. Ocean. Technol.* **2012**, *29* (Suppl. 6), 822–833.

16. Laupattarakasem, P.; Jones, W.L.; Hennon, C.C.; Allard, J.R.; Harless, A.R.; Black, P.G. Improved hurricane ocean vector winds using SeaWinds active/passive retrievals. *IEEE Trans. Geosci. Remote Sens.* **2010**, *48* (Suppl. 7), 2909–2923.

17. Schroeder, L.C.; Jones, W.L.; Boggs, D.H.; Halberstam, I.M.; Dome, G.; Pierson, W.J.; Wentz, F.J. The relationship between wind vector and normalize radar cross section used to derive SeaSat-A satellite scatterometer winds. *J. Geophys. Res.* **1982**, *87*, 3318–3336.

18. Freilich, M.H.; Dunbar, R.S. Derivation of satellite wind model functions using operational surface wind analyses: An altimeter example. *J. Geophys. Res.* **1993**, *98*, 14633–14649.

19. Long, D.G.; Mendel, J.M. Identifiability in wind estimation from scatterometer measurements. *IEEE Trans. Geosci. Remote Sens.* **1991**, *29*, 268–276.

20. Shaffer, S.J.; Dunbar, R.S.; Vincent Hsiao, S.; Long, D.G. A median-filter-based ambiguity removal algorithm for NSCAT. *IEEE Trans. Geosci. Remote Sens.* **1991**, *29*, 167–174.